ACS Macro Letters

Letter

pubs.acs.org/macroletters

Knotting and Unknotting Dynamics of DNA Strands in Nanochannels

Cristian Micheletti*,† and Enzo Orlandini*,‡

†SISSA, International School for Advanced Studies, via Bonomea 265, I-34136 Trieste, Italy

‡Dipartimento di Fisica, Sezione CNISM, and Università di Padova, via Marzolo 8, I-35131 Padova, Italy

Supporting Information

ABSTRACT: The self-knotting dynamics of DNA strands confined in nanochannels is studied with Brownian simulations. The model DNA chains are several microns long and placed inside channels that are 50−300 nm wide. This width range covers the transition between different metric scaling regimes and the concomitant drop of DNA knotting probability for channel widths below ∼75 nm. We find that knots typically originate from deep looping and backfoldings of the chain ends. Upon lowering the channel width, backfoldings become shallower and rarer and the lifetime of knots decreases while that of unknots increases. This lifetimes interplay causes the dramatic reduction of knots incidence for increasing confinement. The results can aid the design of nanochannels capable of harnessing the self-knotting dynamics to quench or relax the DNA topological state as desired.

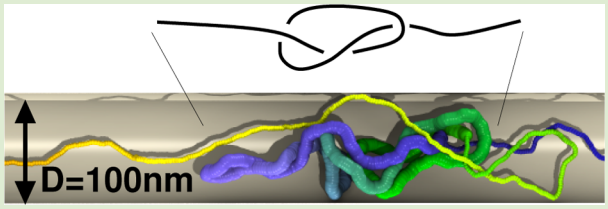

It is only in relatively recent years that experimental and theoretical advancements have allowed for addressing the detailed properties of polymers under spatial confinement and thus reveal a previously unsuspected richness in their physical behavior.[1−11] For these systems, many efforts are still being spent for establishing the impact that self-and mutual chain entanglement, a typical consequence of confinement, have on polymers behavior.[8,12−19] These investigations are largely motivated by the implications of polymer confinement in biological contexts, where it is ubiquitous.

One particular type of entanglement that is drawing much interest in biopolymer contexts is knotting.[17,20−24] In particular, several studies have characterized the equilibrium properties of confined circularized chains in dependence of their topological state. These include the effect of confinement size and dimensionality (spheres,[25,26] slits or slabs,[27−31] channels[32,33]) on the knotting probability of the chains and, in turn, the impact of topology on the chain metric properties. Although physical knots, such as those shown in the graphical abstract, cannot be trapped permanently in chains with free ends, they can still act as long-lived constraints capable of affecting in quantitative tangible ways various chain properties, including metric and mechanical ones.[17−35] Moreover, these "physical knots" can interfere with the elongational process of molecules in nanofluidic devices, an essential prerequisite both for the detection of protein−DNA interactions[36] and for the genome analysis in lab-on-chip experiments.[9] For example, DNA barcoding analysis[37,38] relies on a definite correspondence between the spatial separation of markers in a channel and the genomic distance between two points in the chain, an assumption that is impaired by the presence of knots.

Although the well-characterized equilibrium knotting probability must ultimately originate from the chain internal dynamics, the connection between these two aspects is still largely unexplored.

Here we take a step toward clarifying these issues by investigating, both theoretically and computationally, the dynamical changes of knotted state that spontaneously occur in semiflexible open chains confined inside channels.

This system is an ideal avenue for this endeavor because of the interesting interplay of equilibrium metric and dynamic properties arising in chains subject to quasi one-dimensional confinement.[11,39−41] In this regard we recall that the polymer's longitudinal span (i.e., its extension projected along the channel axis) follows two different asymptotic scaling laws, named after Odijk[42] and de Gennes,[1] according to whether the channel width, D is appreciably smaller or larger than the chain persistence length. For μm long DNA chains, the crossover between these two metric regimes covers the D = 50−100 nm range[8] and is accompanied by a change of the chain internal dynamics, usually detected through the span autocorrelation time.[11,39,41] In the transition region, μm long DNA chains can still sustain major loops and backfoldings[43,44] favoring self-entanglement. In fact, the incidence of physical knots in channel-confined DNA chains is expected to peak in the middle of the transition region and then drop to vanishingly small values for channel widths smaller than about 75 nm.[32]

These observations motivated us to address this transition region and analyze the chain dynamics underpinning the spontaneous formation and untying of knots.

For definiteness, and to relate to feasible experiments, we shall consider model DNA chains of contour length L_c = 3.6 μm and nominal persistence length l_p = 50 nm placed inside channels of diameter D in the 50−300 nm range. This interval of D spans from l_p to about the bulk gyration radius of the chain, R_g^0 nm, thereby realizing the conditions for weak

Received: July 3, 2014
Accepted: August 12, 2014
Published: August 19, 2014

confinement. For each channel width, the Langevin dynamical evolution of the confined open chain is started from a fully elongated, hence unknotted, conformation and followed with up to 4 independent trajectories for a typical total timespan of $310^8\tau_{LJ}$, with the Lennard-Jones time unit, τ_{LJ}, nominally corresponding to 74 ns, see SI.

To solve the ambiguities inherent in the definition, and hence detection, of physical knots in open chains, we used the minimally interfering closure scheme[26] to connect the free ends with a suitable closing arc and then we computed the Alexander determinants to establish the knotted state. Finally, a running-averaging procedure is iteratively applied to remove ephemeral changes of topology over timespans of about $510^4\tau_{LJ}$, see SI. Note that, for simplicity and computational convenience, DNA electrostatic self-interactions are assumed to be completely screened by counterions and hydrodynamic effects in bulk and near the channel walls are neglected.[40] Because of these simplifications, the nominal mapping of simulation time to real time is expected to hold approximately. In fact, the comparison with more detailed models[40] indicates that the nominal time mapping (used hereafter) should be multiplied by about 4 for a more realistic estimate.

Before addressing the entanglement dynamics, we report on the overall chain metric and knotting properties averaged over the Langevin trajectories. The time-averaged quantities shown in Figure 1 are quantitatively consistent with previous Monte Carlo results for an equivalent DNA model[32] and hence support a posteriori the adequate conformational sampling achieved by the collected trajectories, see SI.

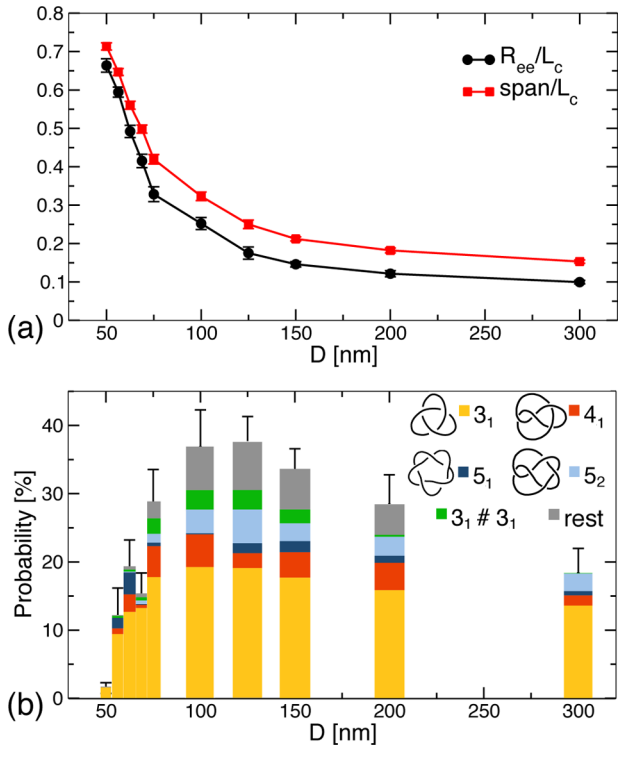

Figure 1. (a) Normalized end-to-end distance and longitudinal span of chains of length L_c = 3.6 μm confined in channels of various width, D. (b) Pile-up histograms for the associated incidence of various knots. As customary, prime knots are labeled by the number of crossings in their simplest representation followed by a conventional indexing subscript. The # sign indicates the composition of prime knots. The indicated errors are calculated from block averaging over intervals of at least 700 ms, which are more than 10× longer than the typical metric autocorrelation time and knot duration at all channel widths, see Figure 3.

As illustrated in Figure 1b, the increase of the chain longitudinal span and end-to-end distance, R_{ee}, upon lowering D is accompanied by the nonmonotonic behavior of the chain knotting probability previously observed in Monte Carlo simulations.[30,20] In particular, one observes a drop of knots incidence for channel widths smaller than about 75−100 nm, that is, well inside the metric crossover region.

Clearly, the equilibrium knotting probability must reflect the ratio of the typical lifetimes of knotted and unknotted states of the confined chains. These two key time scales are, however, not accessible individually in Monte Carlo approaches, which rely on global, non topology-preserving moves.[29,30,32] They can, instead, be separately probed here where the chain dynamics is followed over time scale long enough to observe multiple changes in knotted state at all considered values of D.

This point is aptly illustrated in Figure 2 for a confinement width D = 125 nm (see Figure S2 for a typical knotted configuration at a comparable channel width). The upper panel shows the evolution of the salient chain metric properties together with the highlighting of the knotting events, that are the time intervals during which the chain remains knotted. The major knotting events which last at least 1% of the shown trajectory duration, are further characterized in panel (b). For each event this panel illustrates not only the time evolution of the location of the knot along the chain but also, and most importantly, the frequent changes of knot type that occur during a given knotting event. The most frequent changes of topology, are shown in the graph of panel (c).

By analyzing the succession of knotting events and the time evolution of the metric properties we computed the salient time scales governing the changes of chain geometry and topology, namely, the average autocorrelation time of the longitudinal span, τ_s, and the median duration (or lifetime) of knotted and unknotted states, τ_k and τ_u. The duration of a knotted state is the timespan from the formation of the knot to its untying, that is, the decay to the unknotted state. An analogous definition applies to the unknotted state duration.

The results are summarized in Figure 3. It is seen that the span autocorrelation time peaks at $D \sim 75$ nm and overall covers the nominal time interval of 30−65 ms. Such time scale is comparable to other studies that probed the dynamical behavior of molecules with different contour length, such as the 48.5 kbp long DNA of phage λ. In fact, by using the suggested[41] Rouse-Zimm rescaling of τ_s and accounting for the aforementioned factor of 4 correction, the peak value of τ_s ranges from about 0.5 to 1 s according to whether one uses the bare contour length of λ-DNA (16.5 μm) or the augmented one due to YOYO intercalation (22 μm). These values are consistent with the 0.6−2 s range of peak values of τ_s reported in previous studies on confined λ-DNA.[11,39,41]

Compared to the metric autocorrelation time, τ_s, the time scales associated with the evolution of the topological state cover different timescales over the explored channel widths. Interestingly, the trend of the median knot duration, τ_k, is qualitatively similar to τ_s, featuring a peak at around D = 75 nm followed by a drop by a factor of 2 when D is taken from 75 to 50 nm.

A different behavior, both qualitatively and quantitatively, is seen for the median duration of unknotted states. In fact, τ_u shows an increase, rather than a decrease as the channel width

dx.doi.org/10.1021/mz500402s | ACS Macro Lett. 2014, 3, 876−880

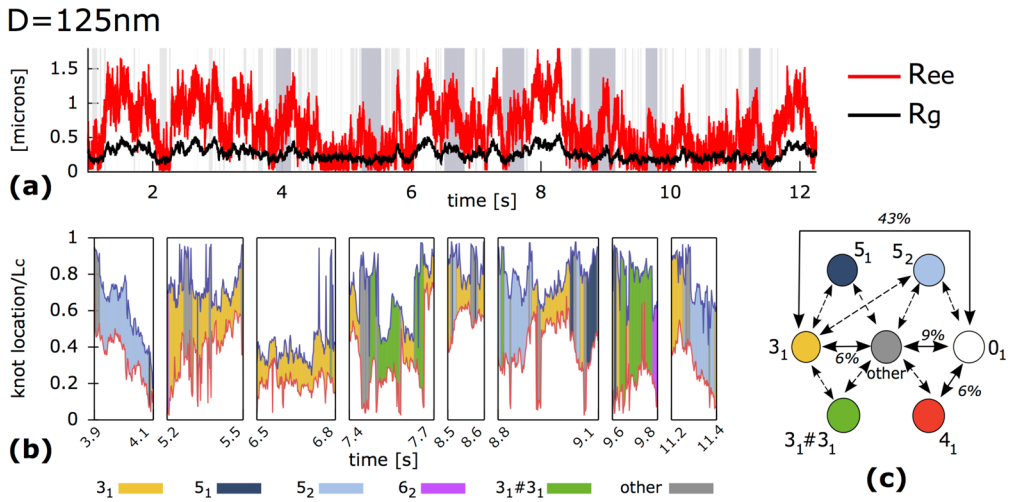

Figure 2. (a) Time evolution of the end-to-end distance, R_{ee}, and gyration radius, R_g, of a 3.6 μm long DNA chain inside a 125 nm wide channel. Gray background bands mark intervals when the chain is knotted. The darker bands reflect knotting events lasting for more than 1% of the shown trajectory duration. Their evolution in terms of knot type and location is given in panel (b). (c) Most common dynamical changes of knot type for the shown trajectory. Their relative statistical weight is shown explicitly if it is larger than 5% and with a dashed line if it is in the 2−5% range. Rarer transitions are not shown. The unknotted state is denoted by 0_1.

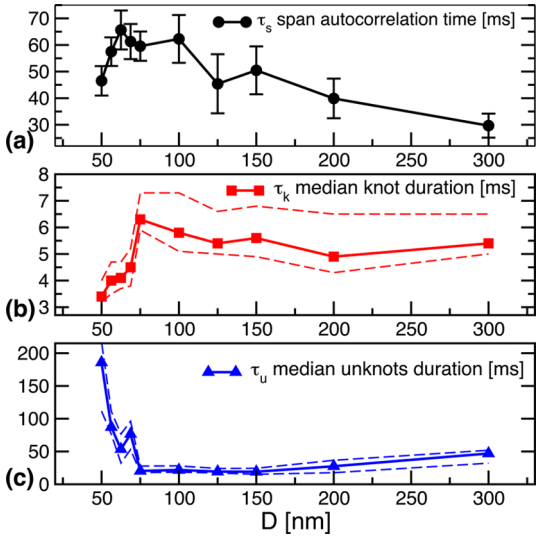

Figure 3. (a) Mean autocorrelation time of the longitudinal span. The error on the mean is calculated from block averaging over intervals of at least 700 ms. The median duration of knots and unknots, τ_k and τ_u, are shown in panels (b) and (c), respectively. The duration distribution width is conveyed by the dashed lines. They correspond to the fifth percentiles on each side of the median. More details about knotted states lifetimes are provided in Figure S4.

is reduced and, more notably, the relative increase going from D = 75 nm down to 50 nm is a factor larger than 10, that is, much larger than the variation of τ_s and τ_k.

The data in Figure 3 therefore clarify that the progressive drop of the knotting probability below D = 75 nm is due to both the decrease of τ_k and the concurrent rise of τ_u, with the latter clearly being the dominant effect.

In addition, the analysis of the simulated trajectories provides valuable insight into the dynamical mechanisms responsible for the steep rise of τ_u which, in fact, can be related to the occurrence of major loops and ends backfolding events.

The influence of end looping on the properties of weakly confined μm long chains has been the subject of several recent investigations.[11,41,43,44] However, their connection with chain self-knotting has not yet been explored. As a matter of fact, creating knots necessitates the presence of loops which must be threaded by one of the chain ends. The specific threading mechanism and loop length can further affect the chain depth at which knots are created.[45]

For $D \sim 70$ nm, the average depth of end loopings, i.e. chain contour length involved in the backfolding of the ends, is about 400 nm and further decreases down to 200 nm at D = 50 nm, see Figure S5. By comparison, the depth of chain backfoldings required to create or untie knots is much larger. This fact emerges from Figure 4, which shows the cumulated probability

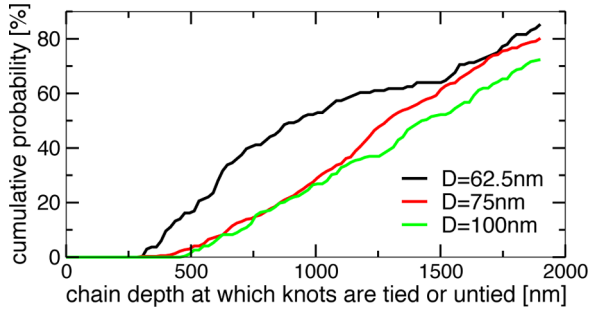

Figure 4. Cumulated probability of the chain depth at which knots are created or untied. The depth is calculated as contour length of the shortest of the two possible terminal segments that comprise the whole knotted region.

distribution for the chain depth at which knots are formed or untied. Knot creation and untying depths are cumulated because of the statistical reversibility of equilibrated Langevin trajectories. In fact, this implies that the role of knot tying and untying events are exchanged in the time-reversed trajectory. The data in Figure 4 show that most knots require deep backfolding of the ends to be formed or untied. In fact, most of knotting events at D = 62.5 nm occur at a chain depth of 800 nm, that is 20% of the contour length. The same point is illustrated by the dynamical evolution in Figure 5 where one can correlate the relatively rare occurrence of knotting events

dx.doi.org/10.1021/mz500402s | ACS Macro Lett. 2014, 3, 876−880

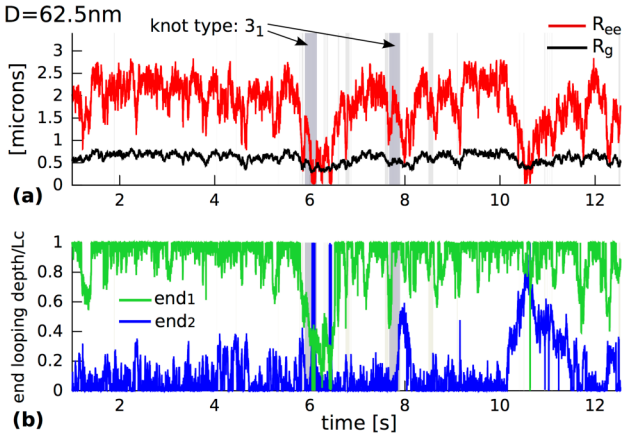

Figure 5. Time evolution of (a) the end-to-end distance and gyration radius and (b) end looping depths of a 3.6 μm long DNA chain inside a 62.5 nm wide channel. For visual clarity the looping depth of one of the two ends is subtracted from 1 (green line). Gray background bands mark intervals when the chain is knotted. The two darker bands reflect knotting events lasting for more than 1% of the trajectory duration, and both involve the formation of a trefoil, 3_1 knot.

with the time evolution of the end looping depth. It is seen that the two major knotting and unknotting events occur in correspondence of atypically large backfoldings of the ends.

The effect remains noticeable even at larger channel widths. In fact, in the D = 125 nm trajectories shown in Figure 2a there is still a noticeable correlation between the onset/termination of long-lived knotting events and the large variations of the end-to-end distance. Furthermore, the comparison of Figures 2a and 5 gives a clear illustration that the lower occurrence of knots in the narrower 62.5 nm wide channel is related to the less frequent incidence of major variations of the end-to-end separation or end looping depth. Indeed, the duration of the major knotting events in the two cases is manifestly similar.

The phenomenology described above allows for rationalizing the interplay of the different metric and topological time scales of Figure 3 within a physically intuitive and appealing framework. In particular, it emerges that the major determinant of the decreasing incidence of knots for D < 75 nm, is the increasingly large waiting time required to produce loops and backfoldings of sufficient depth to favor self-entanglement. Since atypically long loops are required, the duration of unknotted states becomes much larger than the autocorrelation time of the longitudinal span. Finally, the moderate decrease of the depth at which knots are created for increasing confinement further accounts for the observed decrease of the knot duration, τ_k below D = 75 nm. In fact, shallower knots will have a higher chance of reaching by diffusion the nearest end and hence will be shorter lived.

One further and intriguing point regards the relationship of looping and knotting for asymptotically long chains inside channels. The recent study of Muralidhar et al.[46] has shown that, as chain length is increased, the relative difference between span and end-to-end distance tends to vanish. This fact clearly downplays the asymptotic impact on the metric properties of end loopings. However, the fact that backfolding depths grow sublinearly with L_c does neither impair the mechanisms for creating knots nor prevent the average knotting probability to increase with chain. In fact, a loop threading event occurring, for example, at a 300 nm chain depth can create a knot either in a μm long, as considered here, or in a much longer one. At the same time, the average lifetime of knots that are created at a given depth certainly increases with the chain length because knots will survive longer if they do not diffuse toward the nearest end, but toward the farthest one. As a consequence, the knotting probability will increase with chain length for a given channel width, in accord with Monte Carlo results[32] and general arguments borrowed from the proof of the Frisch–Delbruck–Wasserman conjecture.[47]

We conclude by discussing the formation of complex knots through the incremental addition of self-entanglement. This is exemplified by the trajectory in Figure 2b where all major knotting events involve dynamical changes of knot type. It is particularly interesting to notice the occurrence of both prime and composite knots that have an unknotting number larger than one, such as 5_1 and $3_1\#3_1$. These types of knots cannot be tied (or untied) by a single strand passage through a loop, but require multiple instances of elementary knotting (or unknotting) events.

Clearly, this dynamical buildup of knot complexity can occur if the typical duration of knotting events, τ_k, is comparable to the waiting time between loop threading events, which can be approximated by τ_u. Since the difference between τ_u and τ_k diverges for D < 75 nm, the incidence of complex knots should be dramatically reduced below this channel width. This is indeed what is observed in Figure 1 and in the trajectory of Figure 5 where even the major, long-lived knotting events are locked in the simplest, trefoil (3_1), knot type.

To summarize, we used Brownian dynamics simulations to elucidate the mechanisms leading to the spontaneous tying and untying of physical knots in model DNA chains that are confined inside channels of width, D in the 50–300 nm range. We find that most knots are created by deep backfolding or looping of the chain ends. As established also in previous studies,[43,44,41] such backfoldings become rarer and shallower upon reducing D and this, in turn, causes the lifetime of unknots to increase and that of knots to decrease. The resulting interplay of knots and unknots lifetimes causes physical knots to become statistically negligible for D smaller than about 75 nm.

A possible applicative ramification is the tuning of nanochannels fabrication parameters (width and length) so to confine DNA over timespans that are either large or small compared to knots/unknots lifetimes. This ought to allow, respectively, for relaxing or quenching the topological state of the confined DNA (e.g., to minimize knots detrimental effects on DNA barcoding techniques).

■ ASSOCIATED CONTENT

Supporting Information

Additional details of the DNA model, simulation setup, knot detection and localization, and the analysis of various metric and dynamical observables are supplied. This material is available free of charge via the Internet at http://pubs.acs.org.

■ AUTHOR INFORMATION

Corresponding Authors

*E-mail: michelet@sissa.it.
*E-mail: orlandini@pd.infn.it.

Notes

The authors declare no competing financial interest.

■ ACKNOWLEDGMENTS

The authors acknowledge support from the Italian Ministry of Education Grant PRIN 2010HXAW77 and thank Giovanni Bussi and Angelo Rosa for valuable discussions and feedback.

■ REFERENCES

(1) de Gennes, P.-G. *Scaling Concepts in Polymer Physics*; Cornell University Press: Ithaca, NY, 1979.
(2) Tegenfeldt, J. O.; Prinz, C.; Cao, H.; Chou, S.; Reisner, W. W.; Riehn, R.; Wang, Y. M.; Cox, E. C.; Sturm, J. C.; Silberzan, P.; Austin, R. H. *Proc. Natl. Acad. Sci. U.S.A.* **2004**, *101*, 10979−10983.
(3) Stein, D.; van der Heyden, F. H. J.; Koopmans, W. J. A.; Dekker, C. *Proc. Natl. Acad. Sci. U.S.A.* **2006**, *103*, 15853−15858.
(4) Muthukumar, M. *Annu. Rev. Biophys. Biomol. Struct.* **2007**, *36*, 435−450.
(5) Persson, F.; Utko, P.; Reisner, W.; Larsen, N. B.; Kristensen, A. *Nano Lett.* **2009**, *9*, 1382−1385.
(6) Cifra, P.; Bleha, T. *Eur. Phys. J. E: Soft Matter Biol. Phys.* **2010**, *32*, 273−279.
(7) Micheletti, C.; Marenduzzo, D.; Orlandini, E. *Phys. Rep.* **2011**, *504*, 1.
(8) Wang, Y.; Tree, D.; Dorfman, K. *Macromolecules* **2011**, *44*, 6594−6604.
(9) Reisner, W.; Pedersen, J. N.; Austin, R. H. *Rep. Prog. Phys.* **2012**, *75*, 106601.
(10) Dai, L.; Tree, D. R.; van der Maarel, J. R. C.; Dorfman, K. D.; Doyle, P. S. *Phys. Rev. Lett.* **2013**, *110*, 168105.
(11) Tree, D. R.; Wang, Y.; Dorfman, K. D. *Biomicrofluidics* **2013**, *7*, 54118.
(12) Tesi, M. C.; Janse Van Rensburg, E. J.; Orlandini, E.; Whittington, S. G. *J. Phys. A: Math. Gen.* **1994**, *27*, 347−360.
(13) Bonthuis, D. J.; Meyer, C.; Stein, D.; Dekker, C. *Phys. Rev. Lett.* **2008**, *101*, 108303.
(14) Mobius, W.; Frey, E.; Gerland, U. *Nano Lett.* **2008**, 4518−4522.
(15) Tang, J.; Levy, S. L.; Trahan, D. W.; Jones, J. J.; Craighead, H. G.; Doyle, P. S. *Macromolecules* **2010**, *43*, 7368−7377.
(16) Benkova, Z.; Cifra, P. *Macromolecules* **2012**, *45*, 2597−2608.
(17) Marenduzzo, D.; Micheletti, C.; Orlandini, E.; Sumners, D. W. *Proc. Natl. Acad. Sci. U.S.A.* **2013**, *110*, 20081−20086.
(18) Makarov, D. E. *Acc. Chem. Res.* **2009**, *42*, 281−289.
(19) Smeets, R. M. M. S.; Keyser, U. F.; Krapf, D.; Wu, M. Y.; Dekker, N. H.; Dekker, C. *Nano Lett.* **2006**, *6*, 89−95.
(20) Rybenkov, V. V.; Cozzarelli, N. R.; Vologodskii, A. V. *Proc. Natl. Acad. Sci. U.S.A.* **1993**, *90*, 5307−5311.
(21) Meluzzi, D.; Smith, D. E.; Arya, G. *Annu. Rev. Biophys* **2010**, *39*, 349−366.
(22) Grosberg, A. *Polym. Sci., Ser. A* **2008**, *51*, 70−79.
(23) Matthews, R.; Louis, A. A.; Likos, C. N. *ACS Macro Lett.* **2012**, *1*, 1352−1356.
(24) Tang, J.; Ning, D.; Doyle, P. S. *Proc. Natl. Acad. Sci. U.S.A.* **2011**, *108*, 16153−16158.
(25) Micheletti, C.; Marenduzzo, D.; Orlandini, E.; Sumners, D. W. *Biophys. J.* **2008**, *95*, 3591−3599.
(26) Tubiana, L.; Orlandini, E.; Micheletti, C. *Phys. Rev. Lett.* **2011**, *107*, 188302.
(27) Ercolini, E.; Valle, F.; Adamcik, J.; Witz, G.; Metzler, R.; Rios, P. D. L.; Roca, J.; Dietler, G. *Phys. Rev. Lett.* **2007**, *98*, 058102.
(28) Matthews, R.; Louis, A. A.; Yeomans, J. M. *Mol. Phys.* **2011**, *109*, 1289−1295.
(29) Micheletti, C.; Orlandini, E. *Macromolecules* **2012**, *45*, 2113−2121.
(30) Dai, L.; van der Maarel, J. R. C.; Doyle, P. S. *ACS Macro Lett.* **2012**, *1*, 732−736.
(31) Poier, P.; Likos, C. N.; Matthews, R. *Macromolecules* **2014**, *47*, 3394−3400.
(32) Micheletti, C.; Orlandini, E. *Soft Matter* **2012**, *8*, 10959−10968.
(33) Nakajima, C. H.; Sakaue, T. *Soft Matter* **2013**, *9*, 3140−3146.
(34) Matthews, R.; Louis, A. A.; Yeomans, J. M. *Phys. Rev. Lett.* **2009**, *102*, 088101.
(35) Orlandini, E.; Stella, A. L.; Vanderzande, C. *Phys. Biol.* **2009**, *6*, 025012.
(36) Wang, Y. M.; Tegenfeldt, J. O.; Reisner, W. W.; Wang, X. J. *Proc. Natl. Acad. Sci. U.S.A.* **2005**, *102*, 9796−9801.
(37) Lam, E. T.; Hastie, A.; Lin, C.; Ehrlich, D.; Das, S. K.; Austin, M. D.; Deshpande, P.; Cao, H.; Nagarajan, N.; Xiao, M.; Kwok, P.-Y. *Nat. Biotechnol.* **2012**, *30*, 771−776.
(38) Dorfman, K.; King, S. B. W.; Olson, D. W.; Thomas, D.; J. D. R; Tree. *Chem. Rev.* **2013**, *113*, 25842667.
(39) Reisner, W.; Morton, K. J.; Riehn, R.; Wang, Y. M.; Yu, Z.; Rosen, M.; Sturm, J. C.; Chou, S. Y.; Frey, E.; Austin, R. H. *Phys. Rev. Lett.* **2005**, *94*, 196101.
(40) Tree, D. R.; Wang, Y.; Dorfman, K. D. *Phys. Rev. Lett.* **2012**, *108*, 228105.
(41) Chen, Y. L. *Biomicrofluidics* **2013**, *7*, 054119.
(42) Odijk, T. *Macromolecules* **1983**, *16*, 1340−1344.
(43) Cifra, P.; Benková, Z.; Bleha, T. *J. Phys. Chem. B* **2009**, *113*, 1843−1851.
(44) Dai, L.; Ng, S. Y.; Doyle, P. S.; van der Maarel, J. R. C. *ACS Macro Lett.* **2012**, *1*, 1046−1050.
(45) Virnau, P.; Mallam, A.; Jackson, S. *J. Phys.: Condens. Matter* **2011**, *23*, 033101.
(46) Muralidhar, A.; Tree, D.; Wang, Y.; Dorfman, K. *J. Chem. Phys.* **2014**, *140*, 084905.
(47) Sumners, D. W.; Whittington, S. G. *J. Phys. A: Math. Gen.* **1988**, *21*, 1689−1694.